Am J Physiol Lung Cell Mol Physiol 296: L1067–L1075, 2009.
First published April 3, 2009; doi:10.1152/ajplung.00001.2009.

Initiation and maturation of cilia-generated flow in newborn and postnatal mouse airway

Richard J. B. Francis,[1] Bishwanath Chatterjee,[1] Niki T. Loges,[2] Hanswalter Zentgraf,[3] Heymut Omran,[2] and Cecilia W. Lo[1]

[1]*Laboratory of Developmental Biology, National Heart Lung and Blood Institute, National Institutes of Health, Bethesda, Maryland; and* [2]*Department of Pediatrics and Adolescent Medicine, University Hospital Freiburg, Freiburg; and* [3]*Department of Tumor Virology, German Cancer Research Center, Heidelberg, Germany*

Submitted 5 January 2009; accepted in final form 27 March 2009

Francis RJ, Chatterjee B, Loges NT, Zentgraf H, Omran H, Lo CW. Initiation and maturation of cilia-generated flow in newborn and postnatal mouse airway. *Am J Physiol Lung Cell Mol Physiol* 296: L1067–L1075, 2009. First published April 3, 2009; doi:10.1152/ajplung.00001.2009.—Mucociliary clearance in the adult trachea is well characterized, but there are limited data in newborns. Cilia-generated flow was quantified across longitudinal sections of mouse trachea from birth through postnatal day (PND) 28 by tracking fluorescent microsphere speed and directionality. The percentage of ciliated tracheal epithelial cells, as determined by immunohistochemistry, was shown to increase linearly between PND 0 and PND 21 ($R^2 = 0.94$). While directionality measurements detected patches of flow starting at PND 3, uniform flow across the epithelia was not observed until PND 7 at a ~35% ciliated cell density. Flow became established at a maximal rate at PND 9 and beyond. A linear correlation was observed between the percentage of ciliated cells versus flow speed ($R^2 = 0.495$) and directionality ($R^2 = 0.975$) between PND 0 and PND 9. Cilia beat frequency (CBF) was higher at PND 0 than at all subsequent time points, but cilia beat waveform was not noticeably different. Tracheal epithelia from a mouse model of primary ciliary dyskinesia (PCD) harboring a *Mdnah5* mutation showed that ciliated cell density was unaffected, but no cilia-generated flow was detected. Cilia in mutant airways were either immotile or with slow dyssynchronous beat and abnormal ciliary waveform. Overall, our studies showed that the initiation of cilia-generated flow is directly correlated with an increase in epithelial ciliation, with the measurement of directionality being more sensitive than speed for detecting flow. The higher CBF observed in newborn epithelia suggests unique physiology in the newborn trachea, indicating possible clinical relevance to the pathophysiology of respiratory distress seen in newborn PCD patients.

ciliogenesis; development; murine model; primary ciliary dyskinesia; trachea

CILIA-ASSOCIATED DEFECTS are becoming increasingly recognized as playing pivotal roles in a diverse array of pathophysiological processes referred to as ciliopathies (for reviews see Refs. 3, 8). During embryonic development, motile cilia in the node generate nodal flow required for the specification of left-right asymmetry, with disruption or loss of this flow causing defects in laterality (see Ref. 26 for review; Refs. 12, 15, 30). Motile cilia also are important in maintaining normal brain, lung, and reproductive function, as defects in cilia motility can also cause hydrocephalus (12, 13, 15, 16, 29), chronic respiratory disease (21, 28), and infertility (20), respectively.

Address for reprint requests and other correspondence: C. W. Lo, 10 Center Dr., Bldg. 10/Room 6C-103A, MSC-1583, Bethesda, MD 20892 (e-mail: loc@nhlbi.nih.gov).

Primary ciliary dyskinesia (PCD) (MIM no. 242650) is a rare disorder, usually inherited as an autosomal recessive trait. It affects ~1 in 20,000 individuals and is characterized by inborn defects of cilia motility (28). PCD patients often suffer from chronic destructive airway disease due to reduced airway cleaning caused by reduced mucociliary clearance. Approximately half of affected individuals exhibit situs inversus, presumably due to randomization of left-right body asymmetry caused by defects associated with motile cilia at the embryonic node. The association of situs inversus and PCD is also referred to as Kartagener syndrome. Many PCD patients present as neonates with postnatal respiratory distress, which is often misdiagnosed as neonatal pneumonia (28). Interestingly, so far no studies have systematically addressed function of respiratory cilia in neonates.

In the context of a large-scale mouse mutagenesis screen for mutations causing congenital heart disease (33), we recovered several mutant mouse models with phenotypes linked to defects in motile and nonmotile cilia, such as heterotaxy and other laterality defects, hydrocephalus, kidney cysts, and cysts in other organs (Refs. 2, 30, 33; unpublished observations). To evaluate for disruption of cilia motility in these mutants, we assessed ciliary function in the tracheal epithelia as a proxy for motile cilia in the embryonic node or ependymal cilia in the brain (30). Given that many of our mutant mice do not survive long term postnatally because of the severe structural heart defects, the cilia assessments are largely conducted in the airway of neonates or young pups. In contrast to the well-described cilia dynamics and cilia-generated flow in the adult mouse trachea, no information is available on motile cilia function in neonatal mouse trachea (4, 19, 22, 32). Thus the aim of this study was to characterize ciliary motion and cilia-generated flow in the mouse trachea during normal neonatal and early postnatal development.

We examined the emergence of ciliated cells in the airway epithelia in mice from postnatal day (PND) 0 to PND 28 and measured ciliary beat frequency and waveform, using videomicroscopy. Net flow across the epithelia was evaluated by quantitating directionality and speed associated with the movement of fluorescent beads placed in the medium surrounding the tracheal epithelia. We found that directionality measurements were more sensitive than speed measurements for detecting cilia-generated flow, with directionality measurements detecting patches of flow as early as PND 3, while speed measurements failed to detect flow until PND 7. Overall, flow was observed to become established between PND 5 and PND 7, with a epithelial ciliated cell density of 30–35%, and reached a maximal flow state at PND 9 and beyond. Interest-

ingly, cilia beat frequency (CBF) was highest just after birth, possibly an indication of unique physiology associated with the newborn trachea. Using these same approaches, we analyzed ciliary function in an established mouse model of PCD and showed reduced CBF with a shortened stroke and abnormal ciliary waveform (30).

MATERIALS AND METHODS

Mouse breeding and trachea collection. Experiments were conducted in accordance with an animal protocol approved by the Institutional Animal Care and Use Committee of the National Heart, Lung, and Blood Institute (Protocol No. H-0175) with C57BL/6 mice 0–28 PND in age. After euthanasia, trachea were removed in L-15 medium + 10% fetal bovine serum (Invitrogen), cut longitudinally, and either immediately fixed for immunohistochemistry or transferred into a dish for videomicroscopy.

Immunohistochemistry. For immunostaining, tracheas were fixed in 4% paraformaldehyde and secured to a glass coverslip with the tissue adhesive Nexaband (Webster Veterinary) and then permeabilized with PBST (0.2% Triton X-100 in PBS), blocked with 5% goat serum, and incubated overnight at 4°C with an anti-α-tubulin antibody (Sigma). Secondary fluorescent labeling used the anti-mouse Cy3 antibody (Jackson ImmunoResearch Laboratories) diluted in PBST containing Alexa Fluor 488-conjugated phalloidin (5 μl/200 μl; Invitrogen). The tissue was imaged with a Leica DMLFSA microscope with a ×63 water immersion objective and a Hamamatsu ORCA-ER digital charge-coupled device (CCD) camera. Three or four areas (150 μm × 200 μm) were imaged at random along the length of each trachea (n = 5 or 6 trachea per time point) and Z stacks were collected with green fluorescent protein (GFP) and Cy3 filter sets and OpenLab 3.1.7 software (Improvision). Each Z stack was volume deconvoluted and collapsed into a single color image, with the Alexa Fluor 488 and Cy3 images merged for counting ciliated versus nonciliated cells. Mdnah5 staining was conducted as described above on air-dried trachea scrapes with a mouse monoclonal and a rabbit polyclonal produced against the human DNAH5 protein (to amino acid residues 42-325 of DNAH5) (9, 24).

Quantitation of trachea ciliary motility and cilia-generated flow by videomicroscopy. Trachea strips were secured luminal side down on a 35-mm glass-bottomed culture dish (Willco Wells) using a glass coverslip covered with a silicone sheet containing a small window to form a chamber. Cilia dynamics were captured along the edge of the trachea strips at room temperature with a ×100 differential interference contrast (DIC) oil objective and a Leica inverted microscope (Leica DMIRE2), and movies [200 frames/s (fps)] were made with a Phantom v4.2 camera (Vision Research). To quantify CBF, the number of frames required for completion of a single stroke was counted. To quantify flow, 0.20-μm Fluoresbrite microspheres (Polysciences) were added to the trachea bathing medium, and fluorescent movies (15 fps) were collected with FITC filter prisms and a high-speed CCD camera (Hamamatsu, C9100-12). Microsphere speed and directionality were obtained from the movies with Volocity 3.5.1 software (Improvision). For measuring both cilia dynamics and cilia-generated flow three or four randomly selected areas were imaged from five or six trachea per developmental time point, from which up to eight microspheres were tracked per area. Directionality was defined as the net displacement achieved (i.e., the straight line connecting microsphere location in *time point 0* to the last time point measured) divided by the total distance traveled (i.e., the zigzag line collected by tracing microsphere location across all time points); thus a microsphere moving in a straight line would have a directionality of 1, while more random movements approach a directionality of 0.

Immunoblotting. Tracheas were dissected and homogenized (Polytron PT1200) in buffer containing 5 mM PMSF and 1% NP-40 and centrifuged at 12,000 *g* for 10 min at 4°C. The supernatant was then separated on NuPAGE 3–8% Tris-acetate gel (Invitrogen, Karlsruhe, Germany) and blotted onto a polyvinylidene difluoride (PVDF) membrane (Amersham). Immunodetection was carried out with ECL plus (GE Healthcare), with monoclonal and polyclonal anti-DNAH5 made to amino acid residues 42-325 (9, 24).

Data analysis. Data are presented as means ± SD as analyzed with Instat 3 (GraphPad Software) with one-way analysis of variance (ANOVA) and Bonferroni posttest for comparison of all time points. Graphs and linear fit lines were generated/analyzed with Prism 5 (GraphPad Software), with the *F*-test used to determine whether slopes were significantly different from zero.

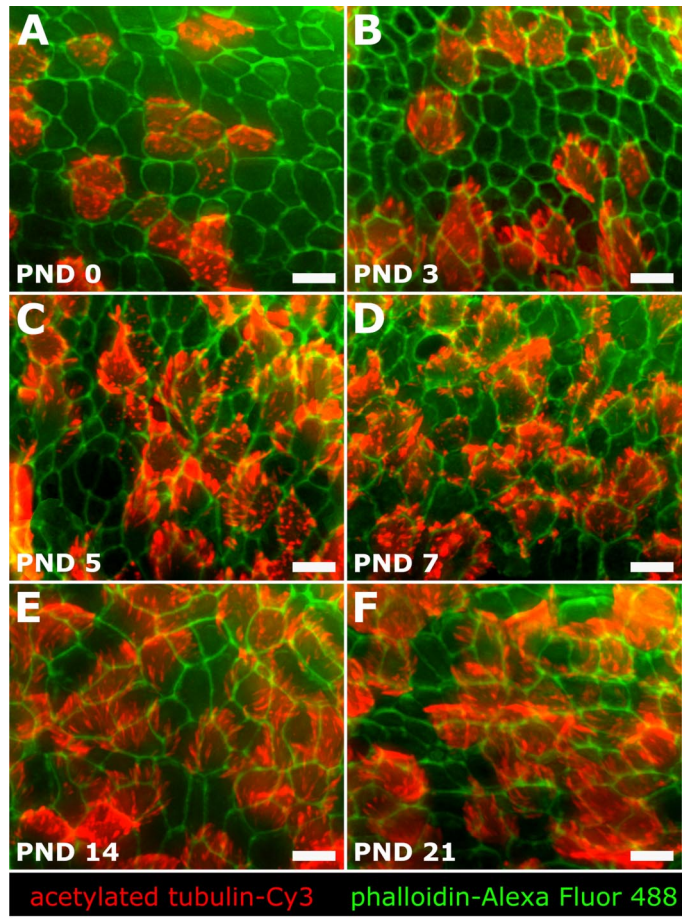

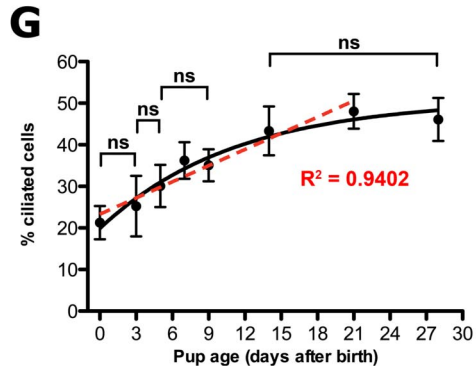

Fig. 1. Postnatal increase in ciliation of the mouse tracheal epithelium. *A–F*: fluorescent immunostaining of the trachea epithelium at postnatal day (PND) 0-21 with Cy3-conjugated acetylated tubulin antibody delineated the cilia (red), while Alexa Fluor 488-conjugated phalloidin delineated the outlines of individual epithelial cells (green). *G*: linear relationship (R^2 = 0.9402) is observed between % of ciliated tracheal epithelium cells and age. Significant differences ($P < 0.05$) were seen between time points unless marked as not significant (ns). Data are presented as means ± SD. Scale bars, 10 μm.

RESULTS

Emergence of ciliated epithelial cells in trachea. Ciliated cells in the mouse tracheal epithelium from birth to PND 28 were visualized with an anti-α-tubulin antibody in conjunction with a fluorochrome-conjugated secondary antibody. Newborn trachea contained few ciliated cells (Fig. 1*A*), but the ciliated epithelial cell density steadily increased with postnatal development (Fig. 1, *A–F*). To quantitate the emergence of ciliated cells, fluorochrome-conjugated phalloidin was used to delineate cell borders in the epithelia, and the percentage of ciliated cells was calculated from the ratio of ciliated cells over total epithelial cells observed per image field. This showed that the density of ciliated cells in the trachea increased linearly after birth, plateauing at PND 14 (Fig. 1*G*). A positive linear correlation ($R^2 = 0.94$, $P = 0.0003$) was observed between the percentage of ciliated cells and postnatal development from birth up to PND 21 (Fig. 1*G*).

Analysis of tracheal flow. To quantify cilia-generated flow, we used videomicroscopy with epifluorescent illumination to visualize the movement of fluorescent microspheres placed in the culture medium bathing the trachea. Digital images were captured at 15 fps to track the movement of individual beads. In newborn tracheal epithelia, the beads did not display coordinated directional movement (Fig. 2*C*; see Supplemental Movie E1) but instead exhibited only random Brownian motion (traces in Fig. 2*C*).[1] Consequently, no net flow was observed. In contrast, similar analysis of PND 14 trachea showed coordinated or directional movement of the beads, with net flow of the beads observed across the tracheal epithelia (traces in Fig. 2*D*; see Supplemental Movie E2).

Quantitation of microsphere motion showed a biphasic distribution for microsphere speed and directionality (Fig. 2, *E* and *F*). Microsphere speed was unchanged from PND 0 to PND 5, followed by a significant increase at PND 7, with a new plateau reached at PND 9 onward (Fig. 2*E*). Microsphere directionality displayed a developmental profile similar to that of speed but was shifted earlier by ~3 days (Fig. 2*F*), with a low plateau 0–3 days after birth, a significant increase at PND 5, and a new plateau reached at PND 7 and onward (Fig. 2*F*).

Examination of speed and directionality histograms revealed that PND 0 microsphere motion (Fig. 3, *A* and *B*) was identical to that observed in control experiments where microspheres were

[1] The online version of this article contains supplemental material.

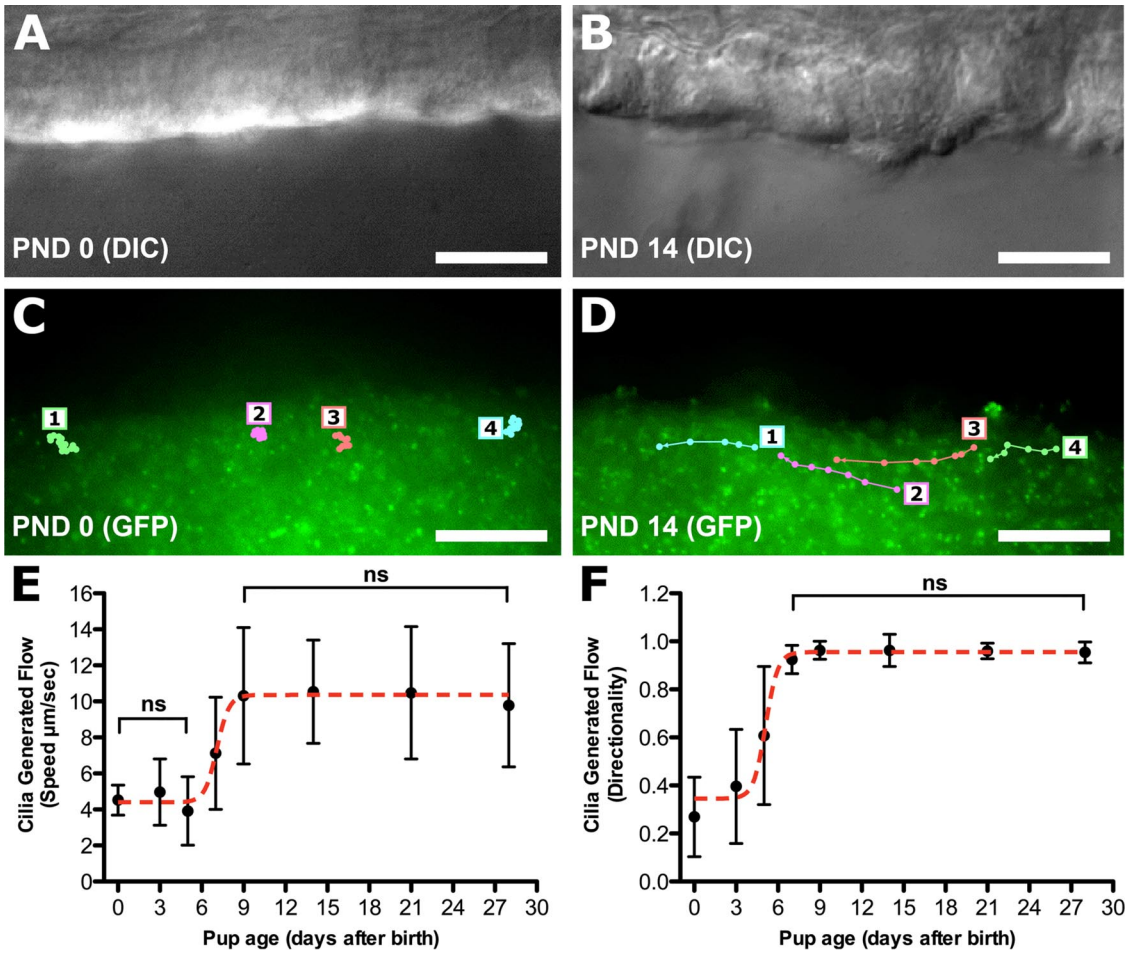

Fig. 2. Measurement of cilia-generated flow in the tracheal epithelium. *A* and *B*: differential interference contrast (DIC) images of PND 0 (*A*) and PND 14 (*B*) tracheal epithelia viewed longitudinally. *C* and *D*: fluorescent 0.20-μm microspheres were added to the tracheal preparation and visualized under epifluorescent illumination. Videomicroscopy was followed by tracing of the movement of 4 individual beads (*1-4*) in the 2 preparations. *E* and *F*: cilia-generated flow was quantified by analyzing the velocity (*E*) and directionality (*F*) of movement associated with the fluorescent microspheres. Significant differences ($P < 0.001$) were seen between time points unless marked as not significant (ns). Data are presented as means ± SD. Scale bars, 10 μm.

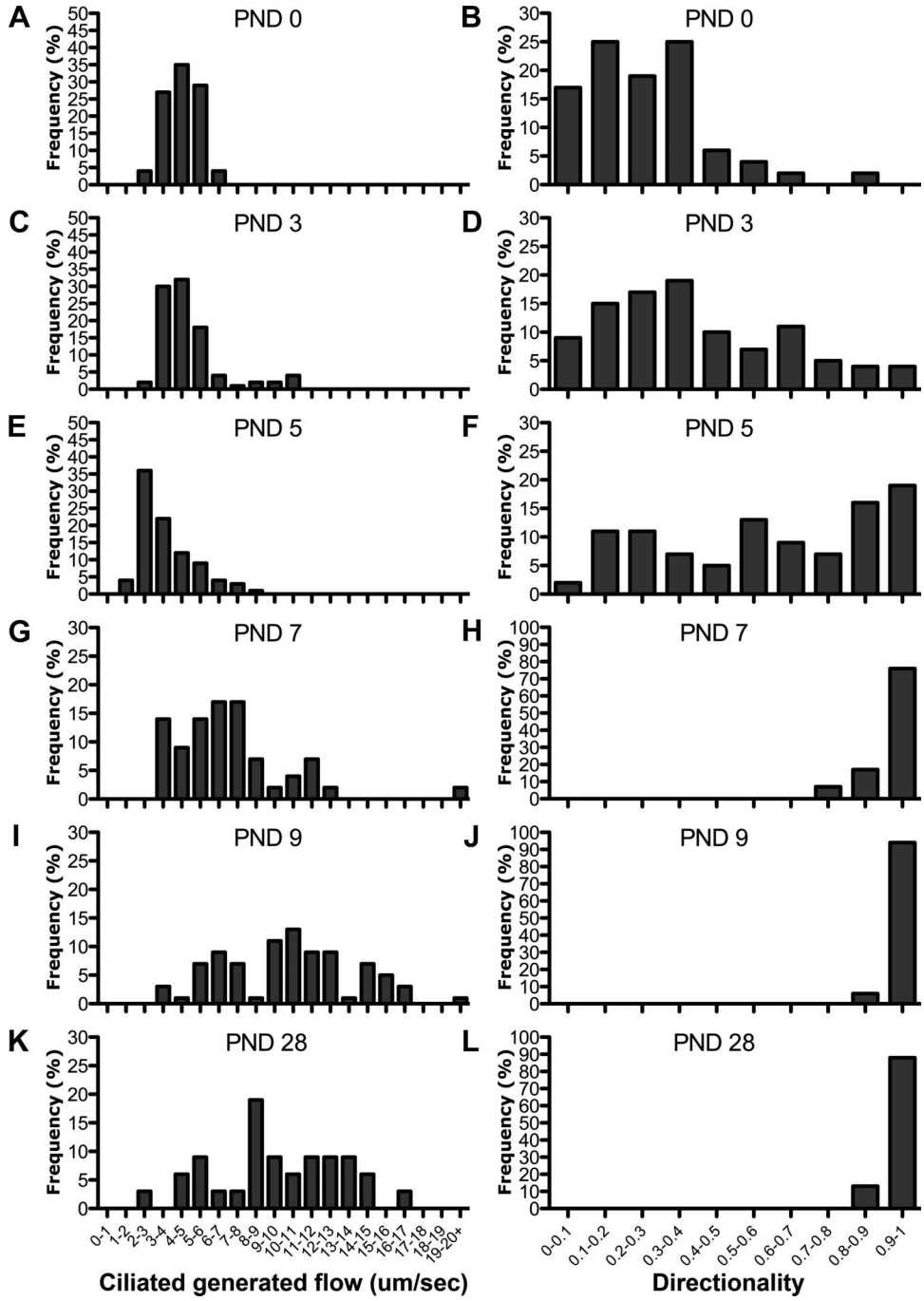

Fig. 3. Histograms of tracheal flow velocity and flow directionality. Distributions of all microsphere speed and directionality measurements are shown (n = 48, 81, 101, 41, 51, 31, for PND 0, 3, 5, 7, 9, and 28, respectively). Note the broadening distribution of speed, while directionality plateaued to maximal flow directionality at PND 7.

placed in medium without any tracheal samples (data not shown). This confirms that the motion observed at PND 0 corresponds to Brownian motion. Speed histograms (Fig. 3) showed a broadening distribution differing from Brownian motion starting at PND 7 (Fig. 3*G*), as flow across the epithelia became established. In contrast, histogram distribution for directionality measurements was already right-shifted at PND 3 (Fig. 3*D*). This corresponds to the emergence of patches of flow in the tracheal epithelia. These results show that flow directionality is more sensitive than flow speed measurements for the detection of cilia-generated flow.

Analysis of cilia waveform and beat frequency. Longitudinal trachea sections used to visualize microsphere motion with epifluorescent illumination were also imaged with standard DIC imaging. This allowed the visualization of ciliary waveform and the quantitation of CBF with images captured at 200 fps by a high-speed camera (Fig. 4; see Supplemental Movie E3). Tracing of cilia beat shape from images obtained from individual ciliated cells at PND 0 (Fig. 4, *A*, *C*, and *D*) and PND 14 (Fig. 4, *B*, *E*, and *F*) showed no difference in their cilia waveforms. Quantitation of CBF showed that while the CBF in embryonic day (E)18.5 embryos and PND 1-2 stage neonates was moderately elevated compared with later stages, there was a significant spike in CBF at birth (PND 0). This was significantly higher compared with all other time points, being

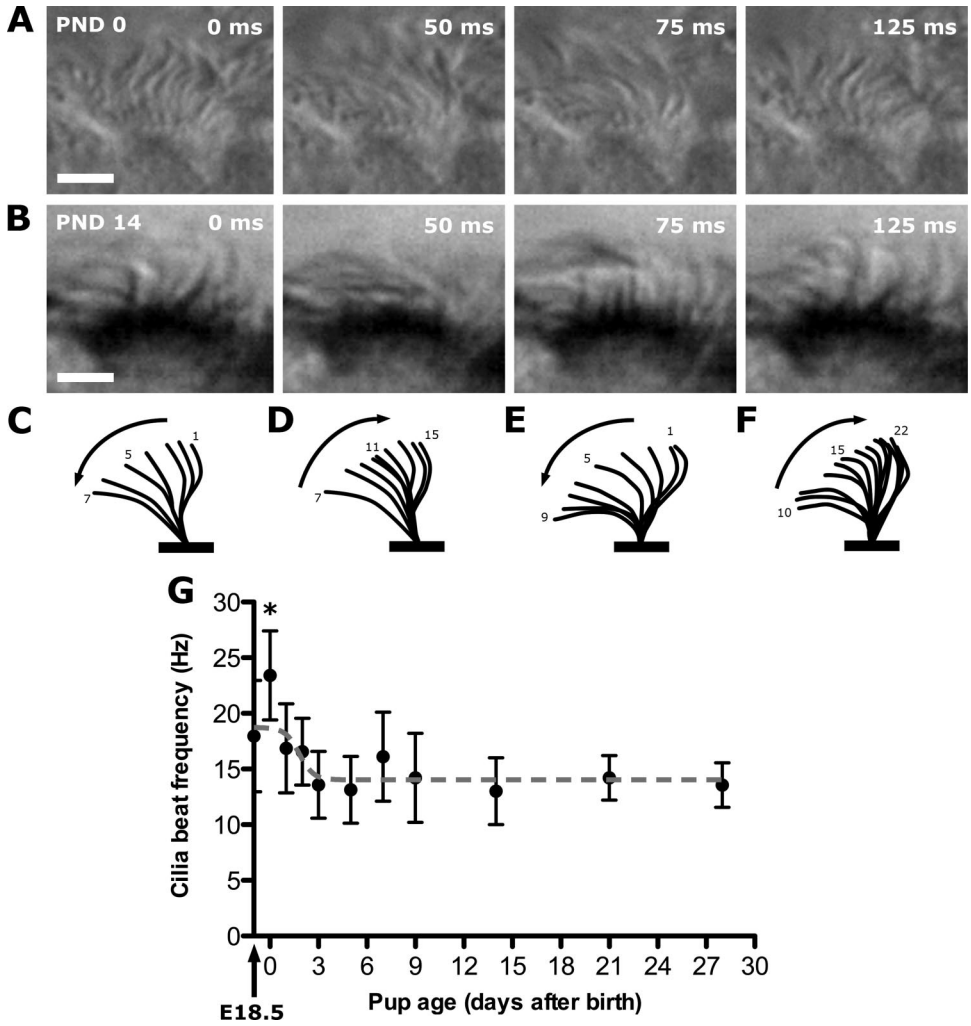

Fig. 4. Cilia waveform and beat frequencies in mouse tracheal epithelia. *A* and *B*: individual frames from movies obtained from PND 0 and PND 14 tracheal epithelia. Scale bars, 5 μm. *C* and *D*: forward and return strokes traced from a single cilia beat cycle at PND 0. *E* and *F*: forward and return strokes traced from a single cilia beat cycle at PND 14. *G*: cilia beat frequency (CBF) was quantified in trachea harvested from near-term embryos [embryonic day (E)18.5] and in mouse neonates between PND 0 and PND 28 in age. While the CBF in E18.5 embryo and PND 1-2 stage neonates was somewhat elevated compared with later stages, only the PND 0 CBF was significantly elevated compared with all other time points (*$P < 0.001$). Data are presented as means ± SD.

23.4 ± 4.4 Hz at birth and then rapidly declining to reach a plateau of 13.6 ± 3.4 Hz at PND 3 onward (Fig. 4*G*).

Cilia-generated flow correlates with increase in ciliated cell density. Our finding that cilia-generated flow in the tracheal epithelia increased with postnatal developmental age is consistent with the increase in the density of ciliated cells in the tracheal epithelia. To determine whether the density of ciliated cells in the epithelia is directly correlated with flow, we plotted percent ciliated cells versus flow speed or flow directionality at PND 0-28 (red lines in Fig. 5) or PND 0-9 (green lines in Fig. 5). Between PND 0 and PND 20, a positive linear correlation was observed between percent ciliated cells and flow speed or directionality ($R^2 = 0.743$, $P = 0.006$ for speed; $R^2 = 0.807$, $P = 0.002$ for directionality) (see red lines in Fig. 5). However, between PND 0 and PND 9, when cilia-generated flow is being established, the correlation of ciliated cell density with speed was weaker ($R^2 = 0.495$, $P = 0.185$), while the correlation with directionality was the strongest ($R^2 = 0.975$, $P = 0.002$) (see green lines in Fig. 5). These results further show that directionality rather than speed is a more sensitive parameter for assessing cilia-generated flow. The plot of directionality vs. percent ciliated cells shows that maximal directionality of 1 is achieved at 35% ciliated cell density, indicating that this is the critical ciliated cell density required for uniform flow across the airway epithelia (Fig. 5*B*).

Abnormal ciliary waveform and no flow in PCD mouse model. Using the flow criteria established in the studies above, we examined tracheal epithelia in a mouse model of PCD with a mutation in *Mdnah5* (alias *Dnahc5*), the ortholog of human DNAH5—the gene most commonly mutated in patients with PCD (11). This mutation, *Mdnah5*$^{del267\text{-}859}$, causes an in-frame deletion of 593 amino acids (residues 267 to 859) that does not include the dynein motor domain in Mdnah5 (30). Homozygous *Mdnah5*$^{del267\text{-}859}$ mice can survive postnatally up to 4 wk of age, eventually expiring because of hydrocephalus (30). We previously showed (28) that this mutation caused an outer dynein arm defect, which is also commonly observed in PCD patients with *DNAH5* mutations.

To better understand the molecular perturbation that underlies the outer dynein arm defect in *Mdnah5*$^{del267\text{-}859}$ mutant mice, we performed immunostaining with monoclonal and polyclonal antibodies directed against the NH_2 terminus (residues 42-328) of human DNAH5 protein. We first demonstrated cross-species specificity of the antibodies by Western blot analyses, which yielded in cell lysates of mouse tracheal epithelia a specific ~500-kDa band, the size range expected for full-length Mdnah5 protein (Fig. 6, *A* and *C*). High-resolution immunofluorescence analyses revealed that in control cells Mdnah5 is specifically expressed in the ciliary axonemes of airway epithelial cells (Fig. 6, *B* and *D*). In the homozygous

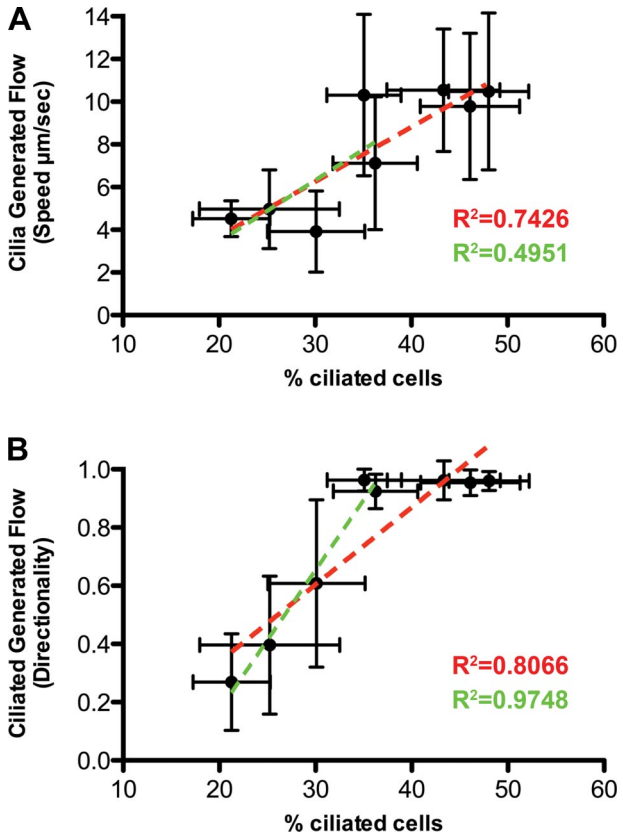

Fig. 5. Ciliated cell abundance correlates with cilia-generated flow in mouse tracheal epithelia. Percentage of ciliated epithelial cells was plotted against flow speed (*A*) or directionality (*B*). Dotted red lines are best fit for PND 0-28, and dotted green lines are best fit for PND 0-9. Directionality shows the best correlation with ciliated trachea epithelia cell number during the initiation of cilia-generated flow between PND 0 and PND 9 ($R^2 = 0.975$), while speed was less well correlated during this same time interval ($R^2 = 0.495$). Data are presented as means ± SD.

Mdnah5$^{del267-859}$ mutant, only low background staining was observed in the ciliary axoneme (Fig. 6, *B* and *D*). This is consistent with previous findings in respiratory cells from PCD patients harboring various recessive loss-of-function *DNAH5* mutations (9). We note that the staining observed in the apical cytoplasm in the area of the microtubule organizing centers or basal bodies also has been observed in respiratory cells of PCD patients with DNAH5 mutations (11). This might reflect abnormal trafficking of mutant DNAH5/Mdnah5 protein or some nonspecific staining.

Videomicroscopy of the tracheal epithelia from PND 3 to PND 28 showed the cilia in these mutants as either immotile or with slow dyssynchronous beat (see Supplemental Movie E4). Examination of the ciliated cell density showed that the percentage of ciliated tracheal cells in homozygous *Mdnah5*$^{del267-859}$ mutants was not different from that in their wild-type littermates (data not shown), but the cilia that were motile displayed a significantly reduced CBF compared with that of wild-type littermates (1.7 ± 1.6 vs. 14.4 ± 4.4 Hz). Quantitation of flow directionality and speed across the trachea of these mutants with fluorescent microspheres showed no evidence of flow at any postnatal developmental time points examined (see Supplemental Movie E5) (Fig. 6, *E* and *F*). Analysis of ciliary motion associated with motile cilia in the mutant epithelia revealed abnormal ciliary waveform with a shortened stroke (Fig. 6*G*; see Supplemental Movie E4).

DISCUSSION

Our studies show that mice are born with few ciliated tracheal epithelia cells, and ex vivo analysis of isolated trachea showed no discernable cilia-generated flow across the tracheal epithelia. Ciliated cell abundance increased linearly after birth, reaching a plateau at PND 14. The progressive increase in epithelial ciliation of the neonatal mouse trachea closely matched the findings of Toskala et al. (31). They showed that cilia first appeared in trachea at E16 and increased until PND 14-21. However, this previous study did not include functional analysis of ciliary motion or cilia-generated flow (31).

Our assessment of cilia-generated flow with fluorescent microspheres showed an increase in flow concurrent with an increase in abundance of ciliated cells in the tracheal epithelia. Microsphere speed and directionality measurements exhibited a biphasic distribution, with no flow observed at birth, followed by the rapid initiation of flow between PND 5 and PND 7 and rising to a plateau at PND 9. We found that histograms of speed and directionality measurements better described the patchy nature of flow observed across the tracheal epithelia. Flow directionality measurements showed patches of flow as early as PND 3, although they were outnumbered by many areas of nonflow. The ratio increased in favor of flow vs. nonflow patches such that by PND 7 flow was observed uniformly across the entire epithelia in all trachea analyzed. In contrast to flow directionality, histograms of flow speed measurements did not detect flow until PND 7.

We found that the initiation of cilia-generated flow was directly correlated with the increase in ciliated cell density, with microsphere directionality rather than speed showing the best correlation. These findings further show that flow directionality is a more sensitive parameter for assessing flow. This reflects the fact that Brownian motion would mask flow at low speeds, which might nevertheless be detectable with the examination of flow directionality. While a number of cilia array studies have previously examined the ability of cilia to generate fluid flow (10, 18), our studies identified that the ~35% ciliated cell density associated with the PND 7 tracheal epithelia is the critical ciliation density required to generate uniform epithelial flow. Although we only examined the tracheal epithelia, our findings are likely to be relevant for flow in the bronchi and bronchioli, because anatomic observations show that ciliated cell density in these airway structures increased in a manner similar to that of the trachea (31). However, as the trachea airway in vivo is coated with a thin layer of higher-viscosity mucus, further studies of cilia-mediated flow using more viscous medium are needed to evaluate how changes in the density of epithelial ciliation may affect mucociliary clearance.

Our findings that cilia-generated flow in the tracheal epithelia emerges over a period of days postnatally led us to reexamine ciliary function in the *Mdnah5*$^{del267-859}$ mutant mouse model of PCD (30). Using videomicroscopy, we previously showed (30) no detectable cilia-generated flow in *Mdnah5*$^{del267-859}$ mutants, although some ciliary motion was observed. In this study, we showed that there is no change in the density of epithelial ciliation in the mutant tracheal epithelia. Examina-

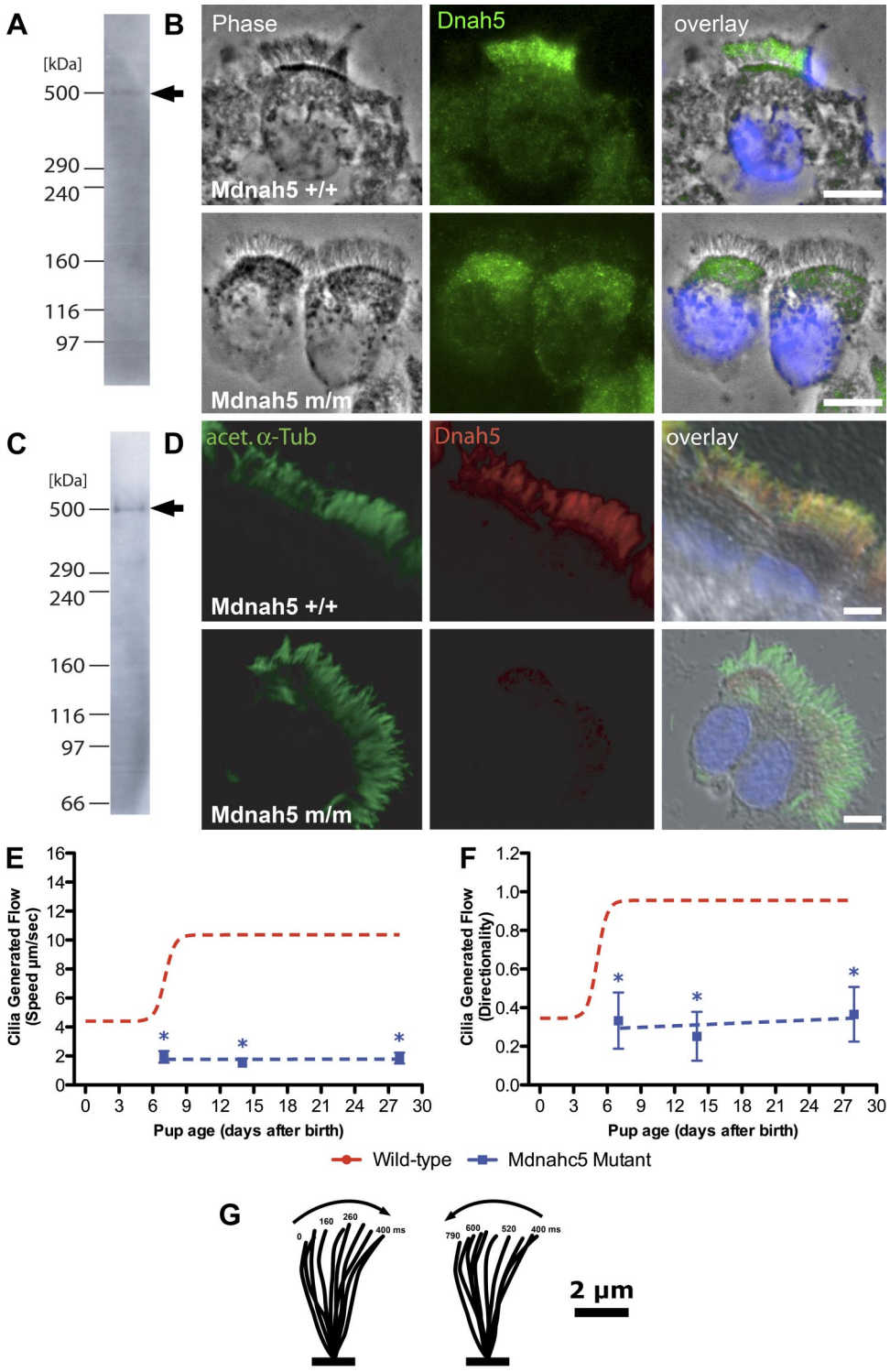

Fig. 6. Airway epithelial cilia of *Mdnah5*$^{del267\text{-}859}$ mutants lack Mdnah5 protein and do not generate epithelial flow. *A–D*: analysis of Mdnah5 expression in tracheal epithelial cells. Immunostaining with a mouse monoclonal (*A*, *B*) or rabbit polyclonal (*C*, *D*) antibody to DNAH5 showed strong staining in the ciliary axoneme of wild-type (+/+) mice. However, the tracheal epithelial cells from homozygous *Mdnah5*$^{del267\text{-}859}$ mutants (m/m) displayed little or no staining in the ciliary axoneme. Specificity of the mouse monoclonal (*A*) and rabbit polyclonal (*C*) antibodies was shown with immunoblotting of extracts from airway epithelia, which showed a band of ~500 kDa (arrows in *A*, *C*), the size range expected for Mdnah5. Scale bars, 5 μm. *E* and *F*: quantitative analysis of cilia-generated flow in *Mdnah5*$^{del267\text{-}859}$ mutants. Cilia-generated flow was quantified by analyzing the speed (*E*) and directionality (*F*) of movement associated with fluorescently labeled microspheres placed above the tracheal epithelia. In homozygous *Mdnah5*$^{del267\text{-}859}$ mutants (blue lines), both the speed and directionality were significantly different (*) from control values (red lines). Data are presented as means ± SD. *G*: tracing of a forward and reverse stroke of cilia from a *Mdnah5*$^{del267\text{-}859}$ mutant epithelial cell obtained using images obtained from a high-speed (200 frames/s) movie. Note absence of the characteristic sweeping motion normally seen in wild-type airway cilia (Fig. 4, *C–F*).

tion of ciliary motion revealed slow dyskinetic movement, with an abnormal ciliary waveform. The cilia beat failed to exhibit the full stroke seen in normal airway cilia motion. Analysis using fluorescent beads showed no net flow generated by the dyssynchronous ciliary beat associated with the mutant airway epithelia. Immunostaining with a DNAH5 antibody suggested that the mutant *Mdnah5* protein, though expressed, is not transported to the ciliary axoneme.

Airway cilia have proved useful as a experimental paradigm to assess the functional roles served by genes known or suspected to encode proteins in the ciliome (12, 16, 17, 29). Our results suggest that measuring cilia-generated flow to assess the potential physiological function of genes in the ciliome would not be possible in mutant mice that die prenatally or neonatally. In such instances, FOXJ1-Cre (34) with the cre/lox system (25) could be used to delete the genes of interest

specifically in the tracheal epithelia, thereby rescuing the prenatal/neonatal lethality.

The lack of cilia-generated flow in newborn tracheas is not due to altered cilia waveform, because our analysis showed that newborn trachea have ciliary waveform or stroke similar to that seen in normal adult mouse airway (16). Rather, the lack of flow is a reflection of the low ciliation cell density in the newborn trachea. While our CBF measurements from PND 3 onward were similar to that of the CBF found in adult mouse airway (4, 6, 17, 29), an unexpected elevation of CBF was seen in the early mouse neonate, which peaked at birth. The finding of elevated CBF in the newborn trachea may represent a higher primitive autonomous CBF displayed by isolated ciliated cells before establishment of metachronal coordination characteristic of mature airway epithelia (27), an idea reminiscent of the autonomous pacemaker activity of isolated myocytes. An alternative explanation is that the sharp CBF peak seen at birth is due to shear stress with fluid clearance and/or perfusion of air into the lungs. Although our data suggest that the airway epithelia of newborn mice are too sparsely ciliated to generate flow, it is interesting to note that human neonates with PCD often develop respiratory distress (7). Thus studies are warranted to assess CBF and ciliation density in the human newborn airway epithelia to ascertain the potential role of cilia-generated flow in the clearance of amniotic fluid from the lungs and its possible contribution to the pathophysiology of neonatal respiratory distress. We note that although clinical studies measuring CBF from nasal biopsies in human subjects have largely not shown any change in CBF with age (1, 5, 14), the youngest infants examined were 5 days old (23).

In conclusion, ex vivo analysis of mouse tracheal epithelia showed that cilia-generated flow is initiated between PND 5 and PND 7, becoming established with maximal flow at PND 9. This is correlated with a linear increase in the density of ciliated tracheal epithelia cells, with ~35% ciliation required for uniform epithelia flow. Our study demonstrates that the most effective use of microspheres for monitoring flow is the measurement of flow directionality rather than speed. Further investigation is needed to examine the efficacy of mucociliary clearance as epithelial ciliation increases with postnatal development. Whether the high CBF observed in newborn mice may have clinical relevance will require further investigation of ciliary density and function in human newborns. Overall, these findings should prove useful for investigating the pathophysiology of ciliopathies involving the airway.

GRANTS

This work was supported by National Heart, Lung, and Blood Institute Grant ZO1-HL-005701.

REFERENCES

1. **Ahmad I, Drake-Lee A.** Nasal ciliary studies in children with chronic respiratory tract symptoms. *Rhinology* 41: 69–71, 2003.
2. **Aune CN, Chatterjee B, Zhao XQ, Francis R, Bracero L, Yu Q, Rosenthal J, Leatherbury L, Lo CW.** Mouse model of heterotaxy with single ventricle spectrum of cardiac anomalies. *Pediatr Res* 63: 9–14, 2008.
3. **Badano JL, Mitsuma N, Beales PL, Katsanis N.** The ciliopathies: an emerging class of human genetic disorders. *Annu Rev Genomics Hum Genet* 7: 125–148, 2006.
4. **Delamanche S, Desforges P, Morio S, Fuche C, Calvet JH.** Effect of oleoresin capsicum (OC) and ortho-chlorobenzylidene malononitrile (CS) on ciliary beat frequency. *Toxicology* 165: 79–85, 2001.
5. **Edwards EA, Douglas C, Broome S, Kolbe J, Jensen CG, Dewar A, Bush A, Byrnes CA.** Nitric oxide levels and ciliary beat frequency in indigenous New Zealand children. *Pediatr Pulmonol* 39: 238–246, 2005.
6. **Elliott MK, Sisson JH, Wyatt TA.** Effects of cigarette smoke and alcohol on ciliated tracheal epithelium and inflammatory cell recruitment. *Am J Respir Cell Mol Biol* 36: 452–459, 2007.
7. **Ferkol T, Leigh M.** Primary ciliary dyskinesia and newborn respiratory distress. *Semin Perinatol* 30: 335–340, 2006.
8. **Fliegauf M, Benzing T, Omran H.** When cilia go bad: cilia defects and ciliopathies. *Nat Rev Mol Cell Biol* 8: 880–893, 2007.
9. **Fliegauf M, Olbrich H, Horvath J, Wildhaber JH, Zariwala MA, Kennedy M, Knowles MR, Omran H.** Mislocalization of DNAH5 and DNAH9 in respiratory cells from patients with primary ciliary dyskinesia. *Am J Respir Crit Care Med* 171: 1343–1349, 2005.
10. **Guirao B, Joanny JF.** Spontaneous creation of macroscopic flow and metachronal waves in an array of cilia. *Biophys J* 92: 1900–1917, 2007.
11. **Hornef N, Olbrich H, Horvath J, Zariwala MA, Fliegauf M, Loges NT, Wildhaber J, Noone PG, Kennedy M, Antonarakis SE, Blouin JL, Bartoloni L, Nusslein T, Ahrens P, Griese M, Kuhl H, Sudbrak R, Knowles MR, Reinhardt R, Omran H.** DNAH5 mutations are a common cause of primary ciliary dyskinesia with outer dynein arm defects. *Am J Respir Crit Care Med* 174: 120–126, 2006.
12. **Ibanez-Tallon I, Gorokhova S, Heintz N.** Loss of function of axonemal dynein Mdnah5 causes primary ciliary dyskinesia and hydrocephalus. *Hum Mol Genet* 11: 715–721, 2002.
13. **Ibanez-Tallon I, Pagenstecher A, Fliegauf M, Olbrich H, Kispert A, Ketelsen UP, North A, Heintz N, Omran H.** Dysfunction of axonemal dynein heavy chain Mdnah5 inhibits ependymal flow and reveals a novel mechanism for hydrocephalus formation. *Hum Mol Genet* 13: 2133–2141, 2004.
14. **Jorissen M, Willems T, Van der Schueren B.** Nasal ciliary beat frequency is age independent. *Laryngoscope* 108: 1042–1047, 1998.
15. **Kennedy MP, Omran H, Leigh MW, Dell S, Morgan L, Molina PL, Robinson BV, Minnix SL, Olbrich H, Severin T, Ahrens P, Lange L, Morillas HN, Noone PG, Zariwala MA, Knowles MR.** Congenital heart disease and other heterotaxic defects in a large cohort of patients with primary ciliary dyskinesia. *Circulation* 115: 2814–2821, 2007.
16. **Lechtreck KF, Delmotte P, Robinson ML, Sanderson MJ, Witman GB.** Mutations in Hydin impair ciliary motility in mice. *J Cell Biol* 180: 633–643, 2008.
17. **Lee L, Campagna DR, Pinkus JL, Mulhern H, Wyatt TA, Sisson JH, Pavlik JA, Pinkus GS, Fleming MD.** Primary ciliary dyskinesia in mice lacking the novel ciliary protein Pcdp1. *Mol Cell Biol* 28: 949–957, 2008.
18. **Lenz P, Ryskin A.** Collective effects in ciliar arrays. *Phys Biol* 3: 285–294, 2006.
19. **Look DC, Walter MJ, Williamson MR, Pang L, You Y, Sreshta JN, Johnson JE, Zander DS, Brody SL.** Effects of paramyxoviral infection on airway epithelial cell Foxj1 expression, ciliogenesis, and mucociliary function. *Am J Pathol* 159: 2055–2069, 2001.
20. **Lyons RA, Saridogan E, Djahanbakhch O.** The reproductive significance of human Fallopian tube cilia. *Hum Reprod Update* 12: 363–372, 2006.
21. **Mall MA.** Role of cilia, mucus, and airway surface liquid in mucociliary dysfunction: lessons from mouse models. *J Aerosol Med Pulm Drug Deliv* 21: 13–24, 2008.
22. **Matsubara E, Nakahari T, Yoshida H, Kuroiwa T, Harada KH, Inoue K, Koizumi A.** Effects of perfluorooctane sulfonate on tracheal ciliary beating frequency in mice. *Toxicology* 236: 190–198, 2007.
23. **O'Callaghan C, Smith K, Wilkinson M, Morgan D, Priftis K.** Ciliary beat frequency in newborn infants. *Arch Dis Child* 66: 443–444, 1991.
24. **Omran H, Kobayashi D, Olbrich H, Tsukahara T, Loges N, Hagiwara H, Zhang Q, Leblond G, O'Toole E, Hara C, Mizuno H, Kawano H, Fliegauf M, Yagi T, Koshida S, Miyawaki A, Zentgraf H, Seithe H, Reinhardt R, Watanabe Y, Kamiya R, Mitchell D, Takeda H.** Ktu/PF13 is required for cytoplasmic pre-assembly of axonemal dynein. *Nature* 456: 611–616, 2008.
25. **Sauer B.** Inducible gene targeting in mice using the Cre/lox system. *Methods* 14: 381–392, 1998.
26. **Shiratori H, Hamada H.** The left-right axis in the mouse: from origin to morphology. *Development* 133: 2095–2104, 2006.
27. **Smith DJ, Gaffney EA, Blake JR.** Modelling mucociliary clearance. *Respir Physiol Neurobiol* 163: 178–188, 2008.
28. **Storm van's Gravesande K, Omran H.** Primary ciliary dyskinesia: clinical presentation, diagnosis and genetics. *Ann Med* 37: 439–449, 2005.

29. **Takaki E, Fujimoto M, Nakahari T, Yonemura S, Miyata Y, Hayashida N, Yamamoto K, Vallee RB, Mikuriya T, Sugahara K, Yamashita H, Inouye S, Nakai A.** Heat shock transcription factor 1 is required for maintenance of ciliary beating in mice. *J Biol Chem* 282: 37285–37292, 2007.
30. **Tan SY, Rosenthal J, Zhao XQ, Francis RJ, Chatterjee B, Sabol SL, Linask KL, Bracero L, Connelly PS, Daniels MP, Yu Q, Omran H, Leatherbury L, Lo CW.** Heterotaxy and complex structural heart defects in a mutant mouse model of primary ciliary dyskinesia. *J Clin Invest* 117: 3742–3752, 2007.
31. **Toskala E, Smiley-Jewell SM, Wong VJ, King D, Plopper CG.** Temporal and spatial distribution of ciliogenesis in the tracheobronchial airways of mice. *Am J Physiol Lung Cell Mol Physiol* 289: L454–L459, 2005.
32. **Winters SL, Davis CW, Boucher RC.** Mechanosensitivity of mouse tracheal ciliary beat frequency: roles for Ca^{2+}, purinergic signaling, tonicity, and viscosity. *Am J Physiol Lung Cell Mol Physiol* 292: L614–L624, 2007.
33. **Yu Q, Shen Y, Chatterjee B, Siegfried BH, Leatherbury L, Rosenthal J, Lucas JF, Wessels A, Spurney CF, Wu YJ, Kirby ML, Svenson K, Lo CW.** ENU induced mutations causing congenital cardiovascular anomalies. *Development* 131: 6211–6223, 2004.
34. **Zhang Y, Huang G, Shornick LP, Roswit WT, Shipley JM, Brody SL, Holtzman MJ.** A transgenic FOXJ1-Cre system for gene inactivation in ciliated epithelial cells. *Am J Respir Cell Mol Biol* 36: 515–519, 2007.